01 Jan 2022

Passive Intermodulation under Different Spring Contact Conditions

Shengxuan Xia

Emmanuel Olugbade

Yuchu He

Yansheng Wang

et. al. For a complete list of authors, see https://scholarsmine.mst.edu/mec_aereng_facwork/4954

Recommended Citation

S. Xia and E. Olugbade and Y. He and Y. Wang and H. Wang and K. Rao and M. Poort and H. Zhou and W. Lee and N. McDonnell and J. Park and C. Hwang, "Passive Intermodulation under Different Spring Contact Conditions," *2022 IEEE International Symposium on Electromagnetic Compatibility and Signal/Power Integrity, EMCSI 2022*, pp. 12 - 16, Institute of Electrical and Electronics Engineers, Jan 2022.
The definitive version is available at https://doi.org/10.1109/EMCSI39492.2022.9889661

2022 IEEE International Symposium on Electromagnetic Compatibility & Signal/Power Integrity (EMCSI) | 978-1-6654-0929-2/22/$31.00 ©2022 IEEE | DOI: 10.1109/EMCSI39492.2022.9889661

Passive Intermodulation Under Different Spring Contact Conditions

Shengxuan Xia[#1], Emmanuel Olugbade[#2], Yuchu He[*3], Yansheng Wang[*4], Hanfeng Wang[*5], Krishna Rao[*6], Marco Poort[*7], Haicheng Zhou[*8], Warren Lee[*9], Nicholas McDonnell[*10], Jonghyun Park[#11], Chulsoon Hwang[#12]
[#]Missouri University of Science and Technology, Rolla, MO, USA
[*]Google LLC, USA
[#1]sx7c3, [#12]hwangc@mst.edu

***Abstract*— Modularized designs have been widely used in today's consumer electronic devices and flexible RF springs are used for electrical connections between the modules. In the meantime, aluminum alloy material becomes a common chassis option. It is well known that the oxidized chassis surface introduces a certain level of nonlinearity when contacted by the springs, as known as passive intermodulation (PIM). PIM is one of the well-known root causes of the RF desensitization (desense). This paper is focused on investigating the relationship between PIM and contact conditions of the springs, especially contact area. The PIM level behavior is explained mathematically by the regrowth rate and the RF power distributions on the contacts. Full-wave simulations and mechanical simulations were conducted to further support the hypothesis.**

Keywords*— *passive intermodulation, radio-frequency interference, spring component, desense, contact area, contact points.

I. Introduction

In modern electronic devices, modularized design is commonly used for massive productions and easy assembly process in factories. Also, it makes the products easy to repair. Thus, there are many different modules in the consumers' electronics. The separate modules need to have the shared ground with the main chassis for the radio frequency (RF) current return path for electromagnetic compatibility or radio frequency interference control purposes. The electrical connections between the modules and the chassis are usually realized by flexible metal components such as springs. The spring-to-chassis contacts, on the one side, the springs are typically gold-plated on their contact tips to have excellent electrical performance. However, on the other side, the chassis surfaces are usually not ideal for electrical contacts due to the oxidization layer on the aluminum alloy surface. Aluminum alloy material is widely used as the chassis because of its inexpensive price, light weight and fair electrical performance, so the non-ideal spring-to-chassis contacts cannot be easily gotten rid of.

Passive intermodulation (PIM) represents a nonlinear behavior between non-ideal metallic contacts. In wireless communication applications in the electronics, due to the nonlinearity, the wide occupied spectrum of the TX signals will inter-modulate and generate the broadband sideband spectrum. The sideband will always follow the TX frequencies and in a frequency-division duplex (FDD) mode, the receiver sensitivity tends to be degraded (desense) due to the spectral regrowth in the sideband spectrum. Furthermore, the TX signal power of the electronic devices can reach up to 23 dBm. Such high transmit power levels will lead to more spectral regrowth in the sideband spectrum which will have a significant adverse impact on the receiver desense performance. Therefore, the study of reducing PIM caused by metallic contact is essential to mitigate desense issues.

PIM generation mechanisms and characterizations have been studied in previous research. One of the most popular mechanisms is the tunnel effect due to the semiconductor-like junction between two metal surfaces [1]. The metal surface tends to form an oxide layer when exposed to air, and a thin oxide layer between the two metal surfaces can generate the PIM. There are other mechanisms for PIM such as the thermal effect. The regrowth rate is an important indicator to differentiate the dominant mechanism for PIM generation [2]. Practically, enlarging the compression force or adding the torque can reduce the amount of PIM generation [3]. An equivalent circuit model was also proposed by [4] based on the understanding of the contact surface topology of the coaxial connectors. For the PIM related topics, great efforts have been spent on the PIM source localizations such as using ultrasound or emission source microscopy [6] [7]. Most of the PIM studies with measurements focus on standard RF components or devices, but seldom do researchers study the non-standard components. It is worthwhile to spend some effort characterizing the PIM in non-standard components such as tiny springs, which are universally used and may have more interesting insights to dig into. For PIM caused by spring contact, previous studies found some interesting phenomena such as the folded structure spring can self-contact itself and cause PIM [8]. Also, statistical study was conducted to investigate the feasibility of using DCR to represent the PIM values [9]. Both studies on springs are mainly focused on the loose contact regions (when the springs barely touch the landing pads) that the PIM levels will have large variations, so the measured data for high-PIM cases can only support some trend analysis.

This material is based upon work supported by Google LLC and the National Science Foundation (NSF) under Grant No. IIP-1916535.

This paper focuses on the PIM performance of firmly contact with low PIM levels. Subtle changes in the PIM level can be well captured in the measurement and all the phenomena can be clearly explained. Due to the regrowth-rate of the inter-products to the carrier frequencies, stable PIM levels can be further reduced in a highly predictable way by spreading the contact to make the RF power to be less concentrated, and the hypothesis is validated with measurement and simulation results.

II. Relationship Between PIM and Contact Area

The nonlinearity of the metallic contact distorts the signals with multiple tones and generate new frequency components named to be the inter-products. To simplify the problem, a two-tone test can be adopted to demonstrate the intermodulation behavior. Assuming there are two sinusoidal waves of different frequencies but with equal amplitude injected into a nonlinear contact point,

$$V_{in}(t) = V_0 \cos 2\pi f_1 t + V_0 \cos 2\pi f_2 t \tag{1}$$

where V_0 is the amplitude of both tones with the frequencies of f_1 and f_2 ($f_1 < f_2$). The linear-nonlinear behavior of a component can usually be represented by the I-V characteristics. The I-V relationship can be expressed by the Taylor series as [9]:

$$I_{in}(t) = a_1 V_{in} + a_2 V_{in}^{\ 2} + a_3 V_{in}^{\ 3} + \cdots \tag{2}$$

When a_1 is the only non-zero coefficient in (2), the component is linear, otherwise, the I-V curve is not a straight line, and the component has nonlinearity. Thus, there will be multiple inter-modulated products but the third-order products (IP_3) usually have the highest amplitude. Also, there exist two sidebands IP_3 occurring at $2f_2 - f_1$ and $2f_1 - f_2$. If the memory effect is not considered [10], the two have equal amplitudes so we can only consider the upper IP_3 which can be expressed as:

$$I_{IP3\_upper} = \tfrac{3}{4} a_3 V_0^3 \cos\left[2\pi(2f_2 - f_1)t\right] \tag{3}$$

From equation (3), it can be clearly observed that the amplitude of the created IP_3 is proportional to the cubical of the amplitude of input tones. Transformed in decibel, this describes a 3 dB/dB changing rate between the input signals and the created IP_3 signals, namely, when the input power is increased/decreased by 1 dB, the IP_3 power will increase/decrease by 3 dB. The description of the changing rate ratio between the input and output is called the regrowth-rate. It is worth noting that the regrowth-rate is constant under low RF power conditions. Under high-power conditions, the regrowth-rate may either have a descending trend (tunneling effect dominates) or a rising trend (thermal effect dominates). In [8], where the same spring-to-pad contacts are studied, the regrowth-rate changed when the TX power exceeded 26 dBm [8]. In this paper, all the studies were conducted below the TX power of 23 dBm to keep the same regrowth-rate.

With the constant regrowth-rate relationship applies, as Fig. 1(a) demonstrated, if the RF signals are injected into one nonlinear contact, a certain level of the IP_3 output is generated as equation (4) states, where α is a constant representing the nonlinearity level of the contact. When the same amount of input power equally distributed and injected into multiple but identical contacts as Fig. 1(b) shows, the input and output power for each branch will be described in (5) (6). The sum of all the outputs from each branch will be (7). Eventually, by changing the contact condition from one contact junction to be N identical contact junctions, the generated IP_3 power satisfies (8).

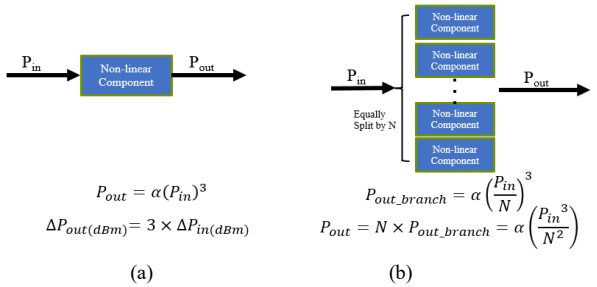

(a) (b)

Fig. 1. Expected IP_3 power for contacts with: (a) single contact point, (b) multiple and identical contact points

$$P_{out} = \alpha \left(P_{in}\right)^3 \tag{4}$$

$$P_{in\_branch} = \frac{1}{N} P_{in} \tag{5}$$

$$P_{out\_branch} = \alpha \left(\frac{P_{in}}{N}\right)^3 \tag{6}$$

$$P_{out}' = N \cdot P_{out\_branch} = \alpha \left(\frac{P_{in}^{\ 3}}{N^2}\right) \tag{7}$$

$$P_{out}'/P_{out} = 1/N^2 \left(\Delta P_{out}(dBm) = 10\log_{10}\left(\frac{P_{out}'}{P_{out}}\right) = -20\log_{10} N\right) \tag{8}$$

Based on the derivations from (4) ~ (8), PIM decreases following a -20 dB/dec rate as the number of the contacts increases. It needs to be mentioned that PIM caused by loosely metal contacts is usually high and unstable. Although the trend can still be roughly captured statistically with the certain figure of merits such as DCR [9], the variations of the measured PIM could be more than 10 dB. However, when there is enough pressure to make sure the springs work in the recommended range, the measured PIM is much more stable. Therefore, measurements can still be used to capture any drastic differences in PIM level.

Similarly, the PIM values can change if the effective contact area changes. If the following two assumptions are valid: a) the RF current flows equally on the effective contact area; b) tightly contact condition (stable PIM), then for an infinitesimal contact area ΔS, the number of the contact counts N_1 and N_2 for the contact area S_1 and S_2 are:

$$N_1 = \frac{S_1}{\Delta S}, \quad N_2 = \frac{S_2}{\Delta S} \tag{9}$$

Based on (4)~(8), if the single contact has an area of ΔS and will generate IP_3 power of P_{out}, then for the cases with contact area S_1 and S_2, the output IP_3 power of these contacts will be:

$$P_{out,1} = P_{out}/N_1^{\ 2} = P_{out}\Delta S^2/S_1^{\ 2}, \; P_{out,2} = P_{out}/N_2^{\ 2} = P_{out}\Delta S^2/S_2^{\ 2} \tag{10}$$

where $P_{out,1}$ and $P_{out,2}$ are the output IP_3 power from the contacts with area S_1 and S_2, respectively. From (10), it can be derived that:

$$\Delta P_{out}(dBm) = 10\log_{10}\left(\frac{P_{out,2}}{P_{out,1}}\right) = 10\log_{10}\left(\frac{S_1^2}{S_2^2}\right) = -20\log_{10}\left(\frac{S_2}{S_1}\right) \quad (11)$$

where ΔP_{out} is output IP_3 power change when the effective contact area is changed from S_1 to S_2. According to equation (11), the PIM level will follow a -20 dB/dec trend to the contact area.

III. Measurement Results and Analysis

The following parts introduce the measurement setup, measured PIM results with different conditions of spring contacts, and the corresponding simulations.

A. Brief Introduction to PIM Measurement Setup

The basic concept of measuring IP_3 generated by the nonlinear contact is to use a two-tone test system based on a low-PIM duplexer (TX: 790~821MHz, RX: 832~863MHz). As Fig. 2 shows, the RF input to the TX port of the duplexer is the combination of high-power two-tone sinusoidal waves. In the measurement, the frequencies of the two tones are 790 and 815 MHz of -22 dBm power from two RF signal generators. Both signal generators are connected to a high-power RF amplifier with 45 dB gain. Then the amplified two sinusoidal signals of 23 dBm (each tone) are combined by the combiner. The "ANT" port of the duplexer is connected to one side of the test fixture and the other side is connected to a 50-ohm low-PIM and high-power dummy load. The design of the test fixture is to have a transmission line structure but insert the spring-to-pad contact in series to the RF path. There are two PCB microstrip lines and one has the spring soldered on the end of the microstrip trace while the other has the pad soldered on the end of the trace. The distance between the two PCBs is precisely controlled by stepper motors. The generated IP_3 is at 840 MHz and will be measured at the "RX" port of the duplexer by a spectrum analyzer. Detailed specifications, RF signal flow paths, and the workflow of the contact measurement have been fully described in [8][9]. The measurement setup adopts the exact design based on the guidelines in [10].

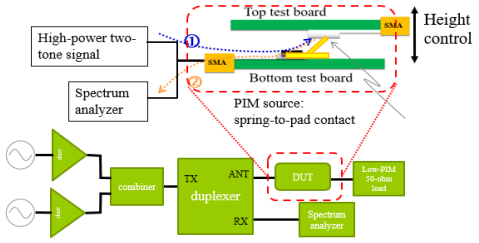

Fig. 2. Two-tone Based PIM measurement system and test vehicle for the spring contact

B. Measured PIM-Discrete Count of Contacts

Three measurements were conducted with the same test setup and fixture. As Fig. 3 (d) shows, only the spring counts at the end of the bottom PCB microstrip trace varied from one to three. PIM, force, height data will be recorded simultaneously during the vertical movement controlled by stepper motors. The measured results for the three cases are shown in Fig. 3 (a) (b) (c) for one, two, and three springs, respectively. Different colors for data points are for the repeating tests (legend notates the iteration number). Since the vertical axis for PIM are all on the same scale, it can be observed that with more springs used, the PIM floor tends to be lower. As we have already emphasized that only the tightly contact PIM (stable PIM) is studied here, to better observe the subtle change of the PIM floor, measured data are zoomed in as shown in Fig. 4. It is worthy to mention that the x-axis height is the top board movement in the vertical direction, in other words, the larger value of the height, the smaller gap between the two PCBs. At the beginning of the movement, when the spring/springs do not make electrical contact with the pad but there are still PIM values measured. Those un-contact PIM values are usually below -100 dBm and caused by the system residue nonlinearity such as the SMA connector. Meanwhile, some data points are not visible in Fig. 4 because they are unstable and have high PIM data out of the observation range. It can be seen in Fig. 4 that when the spring count varies from one (red dashed line) to two (yellow dashed line), the PIM floor decreases by about 6 dB. With three springs, the PIM (deep blue dashed line) has about 3 dB decrease compared to the two springs case (yellow dashed line). Because all the three springs are not evenly mounted, the springs were not landed on the pad at the same height, which caused higher PIM in the height range of 100 um ~ 300 um.

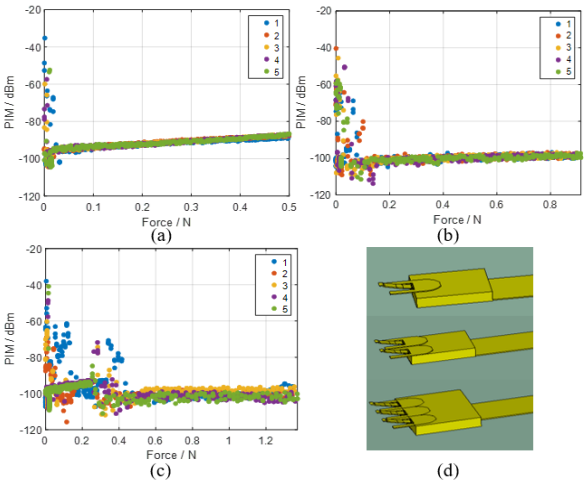

Fig. 3. Measured PIM vs different spring counts. Contact PIM with: (a) single spring (b) double springs (c) triple springs (d) spring counts

To further support the hypothesis that the PIM decrease is caused by the spread of RF concentration of power , full-wave simulations were conducted to investigate the RF current distributions on the springs' tips. As Fig. 5 (a) shows, the two-board with spring-to-pad contact structures were simulated. As shown in Fig. 5 (b) (c) (d), the maximum RF current flowing on the tips of the springs decreases as the spring count increases. As discussed in Section II, when varying the spring counts, the

expected PIM floor change can be calculated by (8). The measured results roughly meet the expectations as Fig. 5 (e) summarizes.

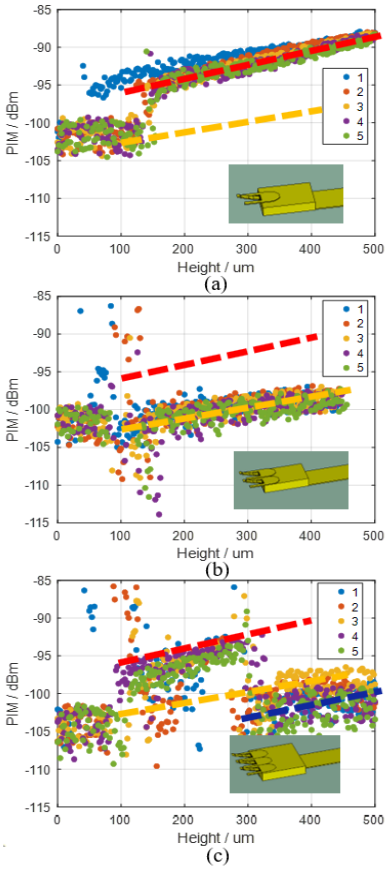

Fig. 4. RF signal flow path in the PIM measurement system: (a) single spring (b) double springs (c) triple springs

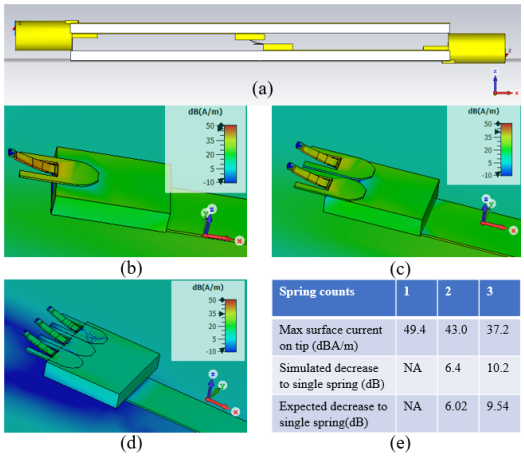

Spring counts	1	2	3
Max surface current on tip (dBA/m)	49.4	43.0	37.2
Simulated decrease to single spring (dB)	NA	6.4	10.2
Expected decrease to single spring(dB)	NA	6.02	9.54

(e)

Fig. 5. CST simulation and results: (a) simulated entire test structure; simulated RF current distribution for (b) single spring (c) double springs (c) triple springs; (e) results summary

C. PIM Floor Change Due to Contact Area Variations

In the measurement results, besides the observations that PIM floor can jump change due to the spring contact count varies, it also can be found that during the compression process, the PIM floors show a slowly rising trend for all the cases. According to the hypothesis that fewer contact points (or smaller contact areas) can increase PIM, if this still applies here to explain the increasing trend of the PIM floor, then according to (11), the effective contact area of the spring keeps decreasing during the compression process. Commonly for a flexible spring, the expectation should be the more compression, the larger the contact area will be made. However, this fork-shaped spring tip has a changing curvature on the surface, which makes it possible that the contact area may even decrease as more deformation is made. To validate this decreasing contact area changing trend and for demonstration of the correctness of (11), mechanical simulation was conducted in ANSYS workbench. In the mechanical simulation, the spring CAD model was imported, and the bottom of the spring was fixed. Another pad was placed in parallel to the spring base and displacement moving towards the spring was gradually proceeded to the pad to mimic the same measurement procedures. As Fig. 6 shows, the contact area first increases with higher loading before 140 um displacement. But 0 ~ 140 um is the unstable PIM range that the spring is loosely connected to the landing pad, so this is not the interested range for discussions. However, the effective contact area does decrease when the spring is further compressed after 140 um displacement.

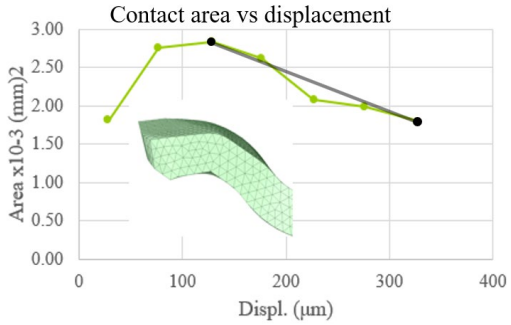

Fig. 6. Mechanical simulation results for contact area change during the compression

The PIM floor change due to the contact area change can be estimated by (11). a) only consider the compression height greater than 140 um range (firmly contact and stable PIM); b) the contact area vs displacement relationship was simplified to be a 2-datapoint linear curve as Fig. 6 black line shows; c) RF current will all go through the tip-to-pad contact and be evenly distributed on the tip. Then based on (11), the expected PIM vs displacement can be expressed as:

$$P_{out(h)}=P_{out}|_{h=140um}+\Delta P_{out(h)}=P_{out}|_{h=140um}-20\log_{10}\left(\frac{S_{(h)}}{S|_{h=140um}}\right)\ (\text{dBm}) \quad (12)$$

where $P_{out}|_{h=140um}$ and $S|_{h=140um}$ are known values for the generated PIM level (in dBm) and the contact area value at the displacement 140um location, respectively. $S_{(h)}$ represents the relationship between contact area and displacement. This is simplified as the black curve in Fig. 6 shows. Applying (12) to

estimate the PIM floor change, the results are shown in Fig. 7 (b) red solid line. The measured results are shown in Fig. 7 (a) and the averaged PIM floor is shown as Fig. 7 (b) blue dashed line.

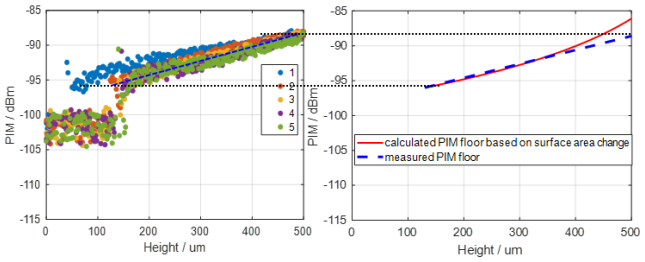

(a) (b)

Fig. 7. Expected IP_3 power change during the compression: (a) measured, (b) estimated with the assumptions

The contact-area-based PIM floor estimations roughly match with what was measured while the discrepancy becomes larger for a deeper press of the spring. However, this is reasonable because when the spring is pressed deeper, the RF current will not only go through the tip-to-pad contact junction but will also have displacement current from the spring body to the pad by capacitive coupling. In other words, as the spring body becomes closer to the pad, more RF current will be distracted by the displacement path, then the assumption c) is no longer valid.

IV. Conclusion

A duplexer-based two-tone test system was used to investigate the lowest PIM (IP_3) level change behavior of non-ideal metallic contacts used frequently in electronic devices. The most important point is that when the inter-products follow the regrowth-rate, the change of the RF power concentration will change the PIM level and all the derivations are originated from the 3 dB/dB regrowth-rate relationship for input power and output IP_3. Spring component with a changing curvature tip was used as the example for demonstration. By varying the contact count number or changing the compression of the spring, the RF power concentration will be changed accordingly and thus result in the change of the PIM. Full-wave EM simulations and mechanical simulations were conducted to further support the hypothesis proposed in this paper. The equation-based estimations are well matched to the measured results for both discrete contacts and the contact area changing case. This study provides a quick but effective insight for PIM suppressions for practical desense problems. In the real design, if the dominant PIM source can be identified, reducing the RF power concentration by adding more contacts or switching to a larger contact can effectively reduce the generated PIM level. The limitation of this solution is that it only applies when the contact is already firm and stable.

References

[1] R. Holm, (1951). The electric tunnel effect across thin insulator films in contacts. *Journal of Applied Physics*, *22*(5), 569–574. https://doi.org/10.1063/1.1700008

[2] J. J. Henrie, A. J. Christianson and W. J. Chappell, "Linear–Nonlinear Interaction and Passive Intermodulation Distortion," *IEEE Transactions on Microwave Theory and Techniques*, vol. 58, no. 5, pp. 1230-1237, May 2010, doi: 10.1109/TMTT.2010.2045527.

[3] Q. Jin, J. Gao, L. Bi and Y. Zhou, "The Impact of Contact Pressure on Passive Intermodulation in Coaxial Connectors," *IEEE Microwave and Wireless Components Letters*, vol. 30, no. 2, pp. 177-180, Feb. 2020, doi: 10.1109/LMWC.2019.2957983.

[4] H. Yang, H. Wen, Y. Qi and J. Fan, "An Equivalent Circuit Model to Analyze Passive Intermodulation of Loose Contact Coaxial Connectors," *IEEE Transactions on Electromagnetic Compatibility*, vol. 60, no. 5, pp. 1180-1189, Oct. 2018, doi: 10.1109/TEMC.2018.2794992.

[5] C. Vicente and H. L. Hartnagel, "Passive-intermodulation analysis between rough rectangular waveguide flanges," *IEEE Transactions on Microwave Theory and Techniques*, vol. 53, no. 8, pp. 2515-2525, Aug. 2005, doi: 10.1109/TMTT.2005.852771.

[6] S. Yang, W. Wu, S. Xu, Y. Zhang, D. Stutts and D. J. Pommerenke, "A Passive Intermodulation Source Identification Measurement System Using a Vibration Modulation Method," *IEEE Transactions on Electromagnetic Compatibility,* vol. 59, no. 6, pp. 1677-1684, Dec. 2017.

[7] S. Yong, S. Yang, L. Zhang, X. Chen, D. J. Pommerenke and V. Khilkevich, "Passive Intermodulation Source Localization Based on Emission Source Microscopy," *IEEE Transactions on Electromagnetic Compatibility*, vol. 62, no. 1, pp. 266-271, Feb. 2020.

[8] J. Li et al., "Self-contact Introduced Passive Intermodulation Characterizations for Captured Springs," *2021 IEEE International Joint EMC/SI/PI and EMC Europe Symposium*, 2021, pp. 929-934, doi: 10.1109/EMC/SI/PI/EMCEurope52599.2021.9559265.

[9] S. Xia et al., "Gassian Process Regression Analysis of Passive Intermodulation Level and DCR for Spring Contacts," *2021 IEEE International Joint EMC/SI/PI and EMC Europe Symposium*, 2021, pp. 935-939, doi: 10.1109/EMC/SI/PI/EMCEurope52599.2021.9559359.

[10] B. Zhang et al., "A Study on the Memory Effect of Mixer," *2020 IEEE Radar Conference (RadarConf20),* 2020, pp. 1-5, doi: 10.1109/RadarConf2043947.2020.9266687.

[11] S. Xia et al., " Practical Fixture Design for Passive Intermodulation Tests for Flexible Metallic Contacts," submitted to *2022 IEEE International Symposium on Electromagnetic Compatibility, Signal & Power Integrity.*